Adaptive-Gain Second-Order Sliding-Mode Control of NPC Converters Via Super-Twisting Technique

Xiaoning Shen, *Member, IEEE*, Chengwei Wu, *Member, IEEE*, Zhuang Liu, *Graduate Student Member, IEEE*, Yijie Wang, *Senior Member, IEEE*, Jose I. Leon, *Fellow, IEEE*, Jianxing Liu, *Senior Member, IEEE*, and Leopoldo G. Franquelo, *Life Fellow, IEEE*

***Abstract*—In this article, a two-stage design approach combining an adaptive-gain generalized super-twisting algorithm (GSTA) and a modified super-twisting observer (STO) is proposed for the three-level neutral-point-clamped (NPC) converters. The key-point of this method is to design some dynamically adapted gains in the standard GSTA, and the tradeoff between dynamic behavior and chattering phenomenon can be addressed. Consequently, the dynamic and steady-state performance of the NPC converter is improved by applying the adaptive-gain GSTA in the power tracking loop and the voltage regulation loop simultaneously. On the other hand, since the convergence rate of the conventional STO is limited while the system trajectories are far away from the origin, a modified STO is applied in the voltage regulator of the NPC converters to reject external disturbances. The finite-time stability of the proposed control scheme is proved. Finally, several comparative experiments are carried out based on a real three-level NPC converter, and the feasibility and effectiveness of the proposed method are validated.**

***Index Terms*—Neutral-point-clamped (NPC) converter, sliding-mode control (SMC), super-twisting observer (STO).**

Manuscript received 27 March 2023; revised 16 July 2023; accepted 2 September 2023. Date of publication 11 September 2023; date of current version 23 October 2023. This work was supported in part by the National Natural Science Foundation of China under Grants 62022030, 62033005, 62373127, and 62320106001, in part by the Fundamental Research Funds for the Central Universities under Grant HIT.OCEF. 2021005, in part by the Heilongjiang Provincial Natural Science Foundation of China under Grant ZD2021F001, in part by the postdoctoral initial funding of Heilongjiang Province under Grants LBH-Q21016 and LBH-Q21097, in part by the Self-Planned Task of State Key Laboratory of Advanced Welding and Joining (HIT) and the Self-Planned Task under Grant SKLRS202215B of State Key Laboratory of Robotics and System (HIT), in part by the Key R&D Program of Heilongjiang Province under Grant 2022ZX01A18, in part by the China Postdoctoral Science Foundation under Grant 2022M720960, and in part by the Heilongjiang Postdoctoral Fund under Grant LBH-Z22119. Recommended for publication by Associate Editor C. K. Tse. *(Corresponding authors: Jianxing Liu; Chengwei Wu.)*

Xiaoning Shen, Chengwei Wu, Zhuang Liu, and Jianxing Liu are with the Department of Control Science and Engineering, Harbin Institute of Technology, Harbin 150001, China (e-mail: xn_shen@hit.edu.cn; chengweiwu@hit.edu.cn; liuz@hit.edu.cn; jx.liu@hit.edu.cn).

Yijie Wang is with the School of Electrical Engineering and Automation, Harbin Institute of Technology, Harbin 150001, China (e-mail: wangyijie@hit.edu.cn).

Jose I. Leon and Leopoldo G. Franquelo are with the ENGREEN Laboratory of Engineering for Energy and Environmental Sustainability, Universidad de Sevilla, 41092 Seville, Spain, and also with the School of Astronautics, Harbin Institute of Technology, Harbin 150001, China (e-mail: jileon@us.es; lgfranquelo@ieee.org).

Color versions of one or more figures in this article are available at https://doi.org/10.1109/TPEL.2023.3313601.

Digital Object Identifier 10.1109/TPEL.2023.3313601

Nomenclature

v_{abc}	$[v_a, v_b, v_c]^T$ AC voltage vector in abc-axis.
i_{abc}	$[i_a, i_b, i_c]^T$ AC current vector in abc-axis.
δ_{abc}	$[\delta_a, \delta_b, \delta_c]^T$ Average duty cycles in abc-axis.
$v_{\alpha\beta}$	$[v_\alpha, v_\beta]^T$ AC voltage vector in $\alpha\beta\gamma$-axis.
$i_{\alpha\beta}$	$[i_\alpha, i_\beta]^T$ AC current vector in $\alpha\beta\gamma$-axis.
$\delta_{\alpha\beta}$	$[\delta_\alpha, \delta_\beta]^T$ Average duty cycles in $\alpha\beta\gamma$-axis.
v_{dc1}, v_{dc2}	Capacitors voltages in the dc side.
v_{dc}	$(v_{dc1} + v_{dc2})$ DC-link voltage.
e_{dc}	$(v_{dc1} - v_{dc2})$ Error between capacitors voltages.
p, p^*	Active power and its reference.
q, q^*	Reactive power and its reference.
C, L, $R_{\rm dc}$	DC-link capacitor, line inductor, and dc load.
ω	AC voltage angular frequency.

I. Introduction

THREE-LEVEL neutral-point-clamped (NPC) active front-end (AFE) converter has become a mature solution for medium-voltage grid-connected applications during the past decades [1], which can be found in motor drives [2], dc microgrids [3], and a variety of renewable energy sources (RESs) [4], [5], [6]. When compared to an equivalent two-level converter, it allows using lower voltage semiconductors for higher power applications, and achieves better power quality as well as smaller common-mode voltage [7].

To achieve stable operation of the three-level NPC converter, the control approaches have become one of the research hotspots in academic areas [8]. In general, the control structure of the NPC can be divided into three loops, that is, the voltage regulation loop (outer loop), power tracking loop (inner loop), and voltage balancing loop [9]. Conventionally, the well-known PI controller is implemented in these loops together with the pulsewidth modulation technique, which has been the most frequently selected solution in industrial applications [10]. However, the control performance of this method is degraded when the system is subject to parameter uncertainties or disturbances [8].

To address this issue, the sliding-mode control (SMC) method is proposed by researchers. The advantageous features including insensitivity to parameter uncertainties and disturbances, fast dynamic and ease of implementation make it widely used in industrial applications [11], [12]. In [13], an SMC controller is proposed to regulate the dc-link voltage for the grid-connected

converters. In [14], a space vector modulation-based SMC control scheme is proposed for the grid-connected NPC converters. However, the performance of the converters suffers from the negative effect of the chattering phenomenon. Then, in [15], the super-twisting algorithm (STA), as one of the second-order SMC methods, is designed in the three-level NPC converter, which not only mitigates the chattering but also preserves the main features of the SMC. In addition, it can also be found in several industrial applications, such as grid-connected ac–dc converters [16], [17] and active power filters [18]. Nevertheless, a drawback of this algorithm is worth to be mentioned, that is, the convergence rate is limited when the system trajectories are far away from the origin, which means the transient response of the converters governed by STA is reduced in this scenario. This issue is addressed by Moreno et al. with a modified STA [19], which is named generalized super-twisting algorithm (GSTA). The GSTA contains extra linear terms, which improves the convergence rate and robustness of the standard STA. In [20], the GSTA is implemented in a underwater vehicle for position tracking, and the applicability of this method is verified by a set of experiments. However, there is a tradeoff between the dynamic performance and the chattering phenomenon when using GSTA.

For the sake of breaking through the aforementioned tradeoff, in this article, an adaptive-gain GSTA is proposed for the grid-connected three-level NPC converters. By introducing dynamically adapted control gains in the standard GSTA, a fast transient response and a reduced chattering phenomenon can be assured simultaneously. As a consequence, the control performance of the three-level NPC converters is enhanced.

On the other hand, it is crucial to ensure a constant dc-link voltage when the NPC converter serves as an AFE in actual applications. However, the unknown external disturbances, such as nonconstant power generated by the RESs in dc microgrids, may induce a voltage fluctuation in the dc-link and endanger the system operation. To address this issue, numerous observer-based feedforward compensation approaches have been reported in the literature [21]. Therein, one representative alternative is the linear extended state observer (LESO), which is the core component of the active disturbance rejection control. It has been applied in the two-level converters and NPC converters to reject external disturbances [15], [22]. However, this method can only achieve asymptotic stability for disturbance estimations (no finite-time convergence) [23]. In [24], a super-twisting observer (STO) is proposed for the grid-connected AFE to reject unknown disturbances, and the estimation errors converge to zero in finite time. Nevertheless, similar to the STA, the estimation speed is limited during a large estimation error, e.g., when a large power is generated by the RESs abruptly in the dc side of the NPC converters.

In this article, inspired by [25], a modified STO is designed for the NPC converter to reject external disturbances. This observer captures the advantages of the STO and LESO simultaneously, which not only achieves finite-time convergence for the disturbances estimation, but also provides a fast estimation speed when a large estimation error appears.

As a consequence, the main contributions of this article can be summarized as follows.

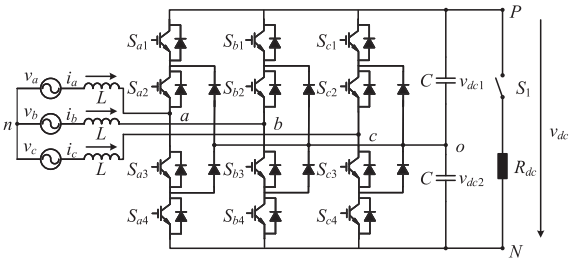

Fig. 1. Three-level NPC converter used as an AFE.

1) An adaptive-gain GSTA is proposed for the NPC converter, which is designed in the voltage regulation loop and power tracking loop simultaneously. By using variable gains in standard GSTA, the adaptive-gain GSTA overcomes the tradeoff between the transient response and the chattering phenomenon, thus, not only assuring the robustness but also improving the dynamic and steady-state performance of the NPC converter. In addition, the corresponding stability analyze is also given.
2) A modified STO is combined with the adaptive-gain GSTA in the voltage regulator to reject external disturbances, which ensures a fast recover of the dc-link voltage when the system is subject to unknown perturbations.
3) A set of comparative experiments including LESO-based STA, STO-based GSTA with different control gains and proposed modified STO-based adaptive-gain GSTA are carried out based a grid-connected NPC converter, and the advantages of the proposed controller is validated.

II. System Model

Fig. 1 depicts a typical structure of the three-level NPC converter used as an AFE. In the ac side, the NPC converter is tied to the grid through three smoothing inductors. In the dc side, two capacitors are used to support the dc-link voltage and to mitigate the high-frequency ripples. By providing a stable voltage for the dc bus, the NPC thereby can be used as an AFE to achieve power exchange with other devices, such as motor drives, RESs, and dc loads. Note that, a nonconstant power generated by these systems may induce voltage fluctuation of dc bus, which can be regarded as an external disturbance. In this work, a dc load is connected to the dc bus to present this scenario.

Assumption 1: The grid voltage in the ac side is balanced.

According to [26], the inductor currents dynamics and capacitor voltages dynamics in $\alpha\beta\gamma$ coordinates are given as

$$L\frac{di_{\alpha\beta}}{dt} = v_{\alpha\beta} - \frac{v_{\rm dc}}{2}\delta_{\alpha\beta} + \frac{e_{\rm dc}}{\sqrt{3}}\begin{bmatrix}\frac{\sqrt{2}(\delta_\beta^2-\delta_\alpha^2)}{4} - \delta_\alpha\delta_\gamma \\ \frac{1}{\sqrt{2}}\delta_\alpha\delta_\beta - \delta_\beta\delta_\gamma\end{bmatrix} \tag{1}$$

$$C\frac{dv_{\rm dc}}{dt} = \delta_{\alpha\beta}^T i_{\alpha\beta} - \frac{2v_{\rm dc}}{R_{\rm dc}} \tag{2}$$

$$C\frac{de_{\rm dc}}{dt} = \frac{1}{\sqrt{6}}\left(i_\alpha\delta_\alpha^2 - i_\alpha\delta_\beta^2 - 2i_\beta\delta_\alpha\delta_\beta\right) + \frac{2\delta_{\alpha\beta}^T i_{\alpha\beta}\delta_\gamma}{\sqrt{3}}. \tag{3}$$

It should be noted that to assure a correct operation of the NPC converter, the capacitor voltages in the dc side must be balanced,

which means the error of capacitor voltages $e_{\rm dc}$ need to be closed to zero. Under this consideration, the inductor currents dynamics deduced in (1) can be approximated as

$$L\frac{di_{\alpha\beta}}{dt} = v_{\alpha\beta} - \frac{v_{dc}}{2}\delta_{\alpha\beta}. \tag{4}$$

III. Controller Design

There are three targets that need to be achieved for the three-level NPC AFE converter, that is, dc-link voltage regulation, instantaneous power tracking, and capacitor voltage balancing. In this work, a cascaded control structure consisting voltage regulation loop, power tracking loop, and voltage balancing loop are adopted to achieve these targets, the control objective of each loop are introduced as the following.

1) In the voltage regulation loop (outer loop), the target is to regulate the dc-link voltage $v_{\rm dc}$ to its reference $v^*_{\rm dc}$, the output of this loop is an active power reference p^* that is employed as the input for the inner loop.
2) In the power tracking loop (inner loop), the active power p and reactive power q must to be controlled to their references p^* and q^*, where p^* can be obtained by the outer loop while q^* is selected according to the requirement.
3) In the voltage balancing loop, it is necessary to assure that the voltage of the two capacitors in the dc side is balanced, i.e., $e_{\rm dc} = v_{\rm dc1} - v_{\rm dc2} \approx 0$. The output of this loop as well as the inner loop will be combined to form the final average duty cycle to regulate the NPC converter.

In this section, the proposed modified STO-based adaptive-gain GSTA control scheme will be introduced in detail. At first, the voltage regulator consisting in a modified STO and an adaptive-gain GSTA is designed. Afterwards, the power tracking loop governed by an adaptive-gain GSTA is presented. Finally, the capacitor voltage balancing loop implemented by a conventional PI controller is introduced.

A. Voltage Regulation Loop

1) Modified STO: A nonconstant power generated by external applications may cause a voltage fluctuation in the dc link of NPC converters, thus, it is necessary to design an observer to compensate this disturbance.

Assumption 2: The dynamic of the power tracking loop is much faster than the dynamic of the voltage regulation loop.

Assumption 2 implies that the dynamic of the power tracking loop can be neglected during the design of voltage regulation loop, which means $p^* \approx p$. Thus, the capacitor voltages dynamics given in (2) can be rewritten as

$$\frac{C}{2}\dot{x}_1 = u_d - x_2, \quad \dot{x}_2 = g(t), \quad y = x_1 \tag{5}$$

where $x_1 = v^2_{\rm dc}/2$, $u_d = p^*$ is the control input, $x_2 = p_r$ is the power consumed by the dc loads, which is regarded as an external disturbance in this article. y is the system output, $g(t)$ denotes the time derivative of x_2, which is bounded by a positive constant G, i.e., $|g(t)| \le G$.

A standard STO can be used to estimate the disturbance, which can be designed as

$$\begin{aligned}\frac{C}{2}\dot{\hat{x}}_1 &= u_d - \hat{x}_2 + k_1 |e_1|^{1/2}\operatorname{sign}(e_1)\\ \dot{\hat{x}}_2 &= -k_2\operatorname{sign}(e_1)\end{aligned} \tag{6}$$

where $e_1 = x_1 - \hat{x}_1$, k_1 and k_2 are the observer gains. Subtracting (6) from (5) yields the dynamic of the estimation errors

$$\begin{aligned}\frac{C}{2}\dot{e}_1 &= -e_2 - k_1 |e_1|^{1/2}\operatorname{sign}(e_1)\\ \dot{e}_2 &= g(t) + k_2\operatorname{sign}(e_1)\end{aligned} \tag{7}$$

where $e_2 = x_2 - \hat{x}_2$. This equation can be represented as following form:

$$\begin{aligned}\dot{z}_1 &= -k_1\sqrt{\frac{2}{C}}|z_1|^{1/2}\operatorname{sign}(z_1) + z_2\\ \dot{z}_2 &= -k_2\operatorname{sign}(z_1) - g(t)\end{aligned} \tag{8}$$

where $z_1 = \frac{C}{2}e_1$ and $z_2 = -e_2$. According to [27], if the observer gains are selected as $k_1 = 0.75\sqrt{2GC}$ and $k_2 = 1.1G$, then the estimation errors e_1 and e_2 will converge to zero in finite time simultaneously, which implies that $x_1 = \hat{x}_1$ and $x_2 = \hat{x}_2$ after a finite time $t > T_s > 0$.

The estimation error of the disturbance can be deduced as

$$e_2 = x_2 - \hat{x}_2 = x_2 + k_2\int_0^t \operatorname{sign}(e_1)dt. \tag{9}$$

Remark 1: It should be pointed out that there is a large estimation error when a large power appears abruptly in the dc side. In this scenario, according to (9), the rate of change of $\hat{x}_2$ is constant, which only depends on the value of k_2. However, a relatively large k_2 may induce high-frequency switching action magnifying measurement noise. For this reason, the value of k_2 cannot be selected too large. Thus, the estimation ability of STO regarding external disturbance is limited in this scenario.

A modified STO proposed in [25] is extended for disturbance estimation in this work to address this issue. By combing STO and LESO, a modified STO for NPC converter can be designed as

$$\begin{aligned}\frac{C}{2}\dot{\hat{x}}_1 &= u_d - \hat{x}_2 + k_1 |e_1|^{1/2}\operatorname{sign}(e_1) + k_3 e_1\\ \dot{\hat{x}}_2 &= -k_2\operatorname{sign}(e_1) - k_4 e_1.\end{aligned} \tag{10}$$

Subtracting (10) from (5), the dynamic of the estimation errors can be derived as

$$\begin{aligned}\frac{C}{2}\dot{e}_1 &= -e_2 - k_1 |e_1|^{1/2}\operatorname{sign}(e_1) - k_3 e_1\\ \dot{e}_2 &= g(t) + k_2\operatorname{sign}(e_1) + k_4 e_1.\end{aligned} \tag{11}$$

This equation can be rewritten as

$$\begin{aligned}\dot{z}_1 &= -k_1\sqrt{\frac{2}{C}}|z_1|^{1/2}\operatorname{sign}(z_1) - \frac{2k_3}{C}z_1 + z_2\\ \dot{z}_2 &= -k_2\operatorname{sign}(z_1) - \frac{2k_4}{C}z_1 - g(t)\end{aligned} \tag{12}$$

where k_3 and k_4 are some positive constants. The finite-time stability of (12) has been proved in [25] if the control gains k_m $(m = 1, \ldots, 4)$ are selected properly. Therefore, it can be concluded that the estimation errors e_1 and e_2 will go to zero in finite time $t > T_e > 0$.

Remark 2: In essence, the modified STO can be regarded as a combination of the STO and LESO, and it inherits the superior features of both. When the system trajectories are far away from the origin, which corresponds to the scenario of large estimation errors, then the modified STO is dominated by the linear terms (LESO), and a fast estimation speed is assured. On the other hand, when the system trajectories are close to the origin, the modified STO is dominated by the nonlinear terms (STO), which provides finite-time stability in this scenario.

Remark 3: The tuning procedures of the modified STO are also introduced to facilitate its implementation in practical engineering applications. Since the modified STO can be regarded as a combination of the STO and LESO, this observer can also be tuned based on the tuning rules of these two observers. The detailed tuning procedures are given as follows.

1) First, a standard STO is tuned. The designed STO is presented in (6), where the parameters k_1 and k_2 need to be tuned. The tuning rules of the STO can be found in [27], [28], and [29], and the gains can be directly selected as
$$k_1 = 0.75\sqrt{2GC}, \quad k_2 = 1.1G. \tag{13}$$
Since the STO is sensitive to measurement noise, the selected parameters should be tested in the actual experimental setup and a simple fine-tune process is required to avoid introducing undesirable noise into the system. At last, the final value of the parameters k_1 and k_2 can be obtained.
2) Second, a standard LESO is tuned. According to the capacitor voltages dynamics given in (5), a standard LESO can be used to estimate the disturbance, which can be designed as
$$\begin{aligned} \frac{C}{2}\dot{\hat{x}}_1 &= u_d - \hat{x}_2 + k_3 e_1 \\ \dot{\hat{x}}_2 &= -k_4 e_1 \end{aligned} \tag{14}$$
where k_3 and k_4 are the observer gains required to tune. The well-known bandwidth-parameterization method is utilized in this work to select the values of k_3 and k_4 [30]. According to the capacitor voltages dynamics and the designed LESO, the estimation errors of the disturbances can be deduced as
$$\begin{bmatrix} \dot{e}_1 \\ \dot{e}_2 \end{bmatrix} = \underbrace{\begin{bmatrix} -\frac{2}{C}k_3 & -\frac{2}{C} \\ k_4 & 0 \end{bmatrix}}_{A} \begin{bmatrix} e_1 \\ e_2 \end{bmatrix} + \begin{bmatrix} 0 \\ 1 \end{bmatrix} g(t) \tag{15}$$
where A is Hurwitz and its characteristic polynomial is given as
$$\lambda^2 + \frac{2}{C}k_3\lambda + \frac{2}{C}k_4 = \lambda^2 + 2\omega_o\lambda + \omega_o^2 = (\lambda + \omega_o)^2 \tag{16}$$
where ω_o is the bandwidth of the ESO, and thus, the observer gains can be selected as $k_3 = C\omega_o, k_4 = C\omega_o^2/2$. At last, similar as the STO, a simple fine-tune process is required in the experimental tests to avoid noise amplification to the system.
3) Finally, the MSTO is tuned based on the aforementioned well-tuned parameters. Applying the MSTO in the actual experimental setup with the well-tuned parameters k_1, k_2, k_3, and k_4. Afterwards, decreasing the value of k_3 and k_4 till the desired performance of the MSTO is achieved.

2) Adaptive-Gain GSTA: In addition to the modified STO, an adaptive-gain GSTA is proposed in the voltage regulation loop to improve the dynamic performance of the NPC converter. The control objective of this loop is to drive the dc-link voltage to its reference value. Under this consideration, the sliding surface s_d is directly selected as
$$s_d = x_1^* - x_1 \tag{17}$$
where $x_1^* = {v_{\rm dc}^*}^2/2$ and $v_{\rm dc}^*$ are the reference of the dc-link voltage. According to the capacitor voltages dynamics (5), the derivative of sliding surface $\dot{s}_d$ can be deduced as
$$\dot{s}_d = -b_d u_d + a_d \tag{18}$$
where $a_d = 2x_2/C$ and $b_d = 2/C$.

The proposed adaptive-gain GSTA is designed as
$$\begin{aligned} u_d &= \alpha_d \phi_1(s_d) + \vartheta_d + \frac{\hat{a}_d}{b_d} \\ \dot{\vartheta}_d &= \beta_d \phi_2(s_d) \end{aligned} \tag{19}$$
where $\hat{a}_d = 2\hat{x}_2/C$ can be estimated by the modified STO introduced in Section III-A, α_d and β_d are the dynamically adapted control gains, which will be designed later
$$\begin{aligned} \phi_1(s_d) &= |s_d|^{\frac{1}{2}} \operatorname{sign}(s_d) + \mu_d s_d \\ \phi_2(s_d) &= \frac{1}{2}\operatorname{sign}(s_d) + \frac{3}{2}\mu_d |s_d|^{\frac{1}{2}} \operatorname{sign}(s_d) + \mu_d^2 s_d \end{aligned} \tag{20}$$
where μ_d is a positive constant. Direct substitution of (19) into (18) yields
$$\begin{aligned} \dot{s}_d &= -\alpha_d b_d \phi_1(s_d) + \omega_d \\ \dot{\omega}_d &= -\beta_d b_d \phi_2(s_d) + \dot{a}_{de} \end{aligned} \tag{21}$$
where $\omega_d = -b_d\vartheta_d + a_{de}$ and $a_{de} = 2e_2/C$.

It should be noted that if the control gains α_d and β_d are selected as some positive constants, (21) turns into a standard GSTA with perturbations [19]. In this work, for the sake of overcoming the tradeoff between dynamic performance and chattering performance, some dynamically adapted control gains are used during the operation. Inspired by [31], the adaptive law is designed as
$$\begin{aligned} \dot{\alpha}_d &= \begin{cases} k_d \operatorname{sign}(|s_d| - w_d), & \text{if } \alpha_d > \alpha_{dm} \\ \eta_d, & \text{if } \alpha_d \le \alpha_{dm} \end{cases} \\ \beta_d &= 2\varepsilon_d \alpha_d \end{aligned} \tag{22}$$

where k_d, w_d, η_d, ε_d, and α_{dm} are some positive constants, and $\alpha_d(0) > \alpha_{dm}$.

Assumption 3: After finite time $t > T_e$, the function $\dot{a}_{de}$ is bounded such that the following conditions are satisfied:

$$|\dot{a}_{de}| \le \delta_{d1} \tag{23}$$

where $\delta_{d1} > 0$ is a positive constant.

Remark 4: The reasonability of *Assumption* 3 in the voltage regulator of NPC converters is discussed. According to the modified STO designed in Section III-A, the estimation error e_2 will converge to zero in finite time. It is noteworthy that the trajectories of system (21) cannot escape to infinity in a finite time [32]. In addition, generally, the observer gains are selected to guarantee that the observation errors converge faster than the controller [27]. Therefore, after finite time $t > T_e$, it can be obtained that e_2 will converge to zero, and it is easy to conclude that there exists a positive constant δ_{d1} such that the following inequality is satisfied:

$$|\dot{a}_{de}| \le \delta_{d1} \tag{24}$$

which implies that *Assumption* 3 holds.

Lemma 1 (see [31]): The adaptive gains α_d and β_d are bounded, and the following inequalities are satisfied:

$$\alpha_d < \alpha_d^*, \beta_d < \beta_d^* \quad \forall t \ge 0. \tag{25}$$

where α_d^* and β_d^* are some positive constants.

Proposition 1: Considering system (21), suppose that Assumption 3 holds, then after finite time $t > T_e$, a 2-sliding mode will be established in finite time via the GSTA (19) with time-varying gains (22).

Proof: The detailed proof of Proposition 1 can refer to the proof of [31, Th. 1], and some details that are different from the proof in [31] are noted in the Appendix. ■

B. Power Tracking Loop

In this loop, the control objective is to drive the active power p and reactive power q to their reference values p^* and q^*. According to the instantaneous power theory, the active and reactive powers in $\alpha\beta\gamma$ coordinates can be given as

$$\begin{aligned} p &= i_{\alpha\beta}^T v_{\alpha\beta} \\ q &= i_{\alpha\beta}^T J v_{\alpha\beta}, \quad J = \begin{bmatrix} 0 & -1 \\ 1 & 0 \end{bmatrix}. \end{aligned} \tag{26}$$

Taking into account the inductor currents dynamics (4), the derivatives of active and reactive powers are derived as follows:

$$\begin{aligned} \dot{p} &= \frac{v_{\alpha\beta}^T}{L}\left(v_{\alpha\beta} - \frac{v_{dc}}{2}\delta_{\alpha\beta}\right) + \omega q \\ \dot{q} &= -\frac{v_{dc}}{2L}\delta_{\alpha\beta}^T J v_{\alpha\beta} - \omega p. \end{aligned} \tag{27}$$

In this loop, a model-based direct power control theory proposed in [26] is used. When the NPC converter is operating correctly in steady state, the active and reactive power track their reference and keep constant, which implies that their first derivative over the time are equal to zero. Solve (27) for this condition yields

$$\delta_{\alpha\beta}^* = \left(\frac{2}{v_{\text{dc}}} + \frac{2\,L\omega q}{v_{\text{dc}}\|v_{\alpha\beta}\|^2}\right) v_{\alpha\beta} - \left(\frac{2\,L\omega p}{v_{\text{dc}}\|v_{\alpha\beta}\|^2}\right) J v_{\alpha\beta} \tag{28}$$

where $\|v_{\alpha\beta}\|^2 = v_\alpha^2 + v_\beta^2$, $\delta_{\alpha\beta}^*$ is the average duty cycle in steady state, that is, the so-called equilibrium point. Then, the control target turns into driving the system to the equilibrium point, and the control input is presented as [26]

$$\delta_{\alpha\beta} = \delta_{\alpha\beta}^* - u(s_p)v_{\alpha\beta} - u(s_q)Jv_{\alpha\beta} \tag{29}$$

where $u(s_p)$ is the controller of active power while $u(s_q)$ is the controller of reactive power, $s_p = p^* - p$ and $s_q = q^* - q$ are the tracking errors of active and reactive powers, which are also selected as the sliding surfaces.

In this loop, the proposed adaptive-gain GSTA is applied to regulate the active and reactive powers, and the controllers are designed as

$$\begin{aligned} u(s_p) &= \alpha_p \phi_1(s_p) + \vartheta_p \\ \dot{\vartheta}_p &= \beta_p \phi_2(s_p) \end{aligned} \tag{30}$$

and

$$\begin{aligned} u(s_q) &= \alpha_q \phi_1(s_q) + \vartheta_q \\ \dot{\vartheta}_q &= \beta_q \phi_2(s_q) \end{aligned} \tag{31}$$

where α_i and β_i $(i = p, q)$ are the adaptive gains, which are given as

$$\begin{aligned} \dot{\alpha}_i &= \begin{cases} k_i \operatorname{sign}(|s_i| - w_i), & \text{if } \alpha_i > \alpha_{im} \\ \eta_i, & \text{if } \alpha_i \le \alpha_{im} \end{cases} \\ \beta_i &= 2\varepsilon_i \alpha_i \end{aligned} \tag{32}$$

where k_i, w_i, η_i, ε_i, and α_{im} are some positive constants, and $\alpha_i(0) > \alpha_{im}$. The functions $\phi_1(s_i)$ and $\phi_2(s_i)$ can be presented as

$$\begin{aligned} \phi_1(s_i) &= |s_i|^{\frac{1}{2}} \operatorname{sign}(s_i) + \mu_i s_i \\ \phi_2(s_i) &= \frac{1}{2}\operatorname{sign}(s_i) + \frac{3}{2}\mu_i |s_i|^{\frac{1}{2}} \operatorname{sign}(s_i) + \mu_i^2 s_i \end{aligned} \tag{33}$$

where μ_i are some positive constants.

By solving (27), (28), and (29), the time derivatives of the sliding surfaces $\dot{s}_p$ and $\dot{s}_q$ can be deduced as

$$\begin{aligned} \dot{s}_p &= a_p - b_{pq} u(s_p) \\ \dot{s}_q &= a_q - b_{pq} u(s_q) \end{aligned} \tag{34}$$

where $a_p = \dot{p}^*$, $a_q = \dot{q}^*$, and $b_{pq} = \frac{v_{dc}\|v_{\alpha\beta}\|^2}{2\,\text{L}}$. Afterwards, by substituting (30) and (31) into (34), $\dot{s}_p$ and $\dot{s}_q$ can be rewritten as

$$\begin{aligned} \dot{s}_p &= -\alpha_p b_{pq} \phi_1(s_p) + \omega_p \\ \dot{\omega}_p &= -\beta_p b_{pq} \phi_2(s_p) + \dot{\chi}_p \end{aligned} \tag{35}$$

and

$$\begin{aligned} \dot{s}_q &= -\alpha_q b_{pq} \phi_1(s_q) + \omega_q \\ \dot{\omega}_q &= -\beta_q b_{pq} \phi_2(s_q) + \dot{\chi}_q \end{aligned} \tag{36}$$

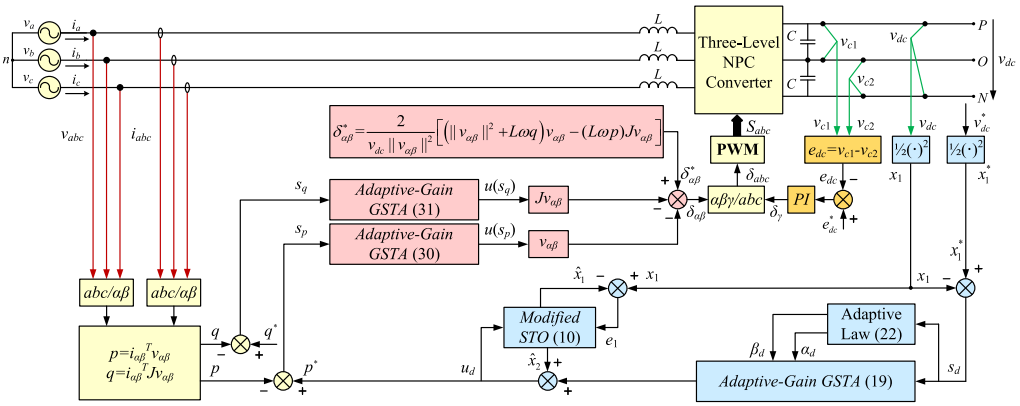

Fig. 2. Control block diagram of proposed modified STO-based adaptive-gain GSTA control scheme for the three-level NPC converter.

where $\omega_i = -b_{pq}\vartheta_i + a_i$ and $\dot{\chi}_i = -\dot{b}_{pq}\vartheta_i + \dot{a}_i$, $(i = p, q)$.

Assumption 4: The functions $\dot{\chi}_i$ $(i = p, q)$ are bounded by some positive constants δ_{i2}, respectively, $(|\dot{\chi}_i| \le \delta_{i2})$ on any finite-time interval.

Remark 5: The reasonability of *Assumption* 4 in the power tracking loop of NPC converters is discussed. On the one hand, the function $\|v_{\alpha\beta}\|^2 = v_\alpha^2 + v_\beta^2$ is constant under balanced grid conditions. On the other hand, according to the dc-link voltage dynamic given in (2), it is easy to conclude that $\dot{v}_{dc}$ is bounded. Therefore, there always exists a positive constant B such that $|\dot{b}_{pq}| \le B$. In addition, when the NPC converter is operated correctly, the functions $\dot{a}_p = \ddot{p}^*$ and $\dot{a}_q = \ddot{q}^*$ are bounded with a positive constant F according to [12]. Additionally, there exists some upper bounds β_i^* $(i = p, q)$ of the adaptive gains β_i according to *Lemma* 1. Thus, it can be deduced that

$$|\dot{\chi}_i| \le B\beta_p^* \int_0^t \left(\frac{1}{2} + \frac{3}{2}\mu_i |s_i|^{\frac{1}{2}} + \mu_i^2 |s_i|\right) d\tau + F, \quad i \in \{p, q\}. \tag{37}$$

Since s_p and s_q are bounded in actual power converters, there always exists two constants δ_{p2} and δ_{q2} such that the following inequalities are satisfied on any finite-time interval:

$$|\dot{\chi}_i| \le \delta_{i2}, \quad i \in \{p, q\} \tag{38}$$

which means *Assumption* 4 holds.

Proposition 2: Taking into account systems (35) and (36), suppose that *Assumption* 4 holds, then the 2-sliding modes will be established in finite time via the GSTAs (30) and (31) with time-varying gains (32).

The proof of Proposition 2 is omitted since it is similar as the proof of Proposition 1.

C. Voltage Balancing Loop

The control objective of this loop is to assure that the voltages of two capacitors in the dc side are balanced, i.e., $e_{\rm dc} = v_{\rm dc1} - v_{\rm dc2} \approx 0$.

Assumption 5: The dynamics of the instantaneous power are much faster than the dynamics of the $e_{\rm dc}$.

Taking into account *Assumption* 5, the instantaneous power can be considered as operating at equilibrium point during the design of voltage balancing loop. Substituting (28) into (3), the capacitor voltages dynamics can be presented as

$$\dot{e}_{\rm dc} = \frac{4p^*}{\sqrt{3}v_{\rm dc}C}\delta_\gamma + \varpi(t) \tag{39}$$

where

$$\varpi(t) = \frac{1}{\sqrt{6}C}\left[(\delta_\alpha^*)^2 i_\alpha - (\delta_\beta^*)^2 i_\alpha - 2\delta_\alpha^*\delta_\beta^* i_\beta\right]. \tag{40}$$

In this loop, a conventional PI controller is used to achieve voltage balancing effectively. The controller is designed as

$$\delta_\gamma = k_{pb}\left(e_{\rm dc}^* - e_{\rm dc}\right) + k_{ib}\int_0^t \left(e_{\rm dc}^* - e_{\rm dc}\right) d\tau. \tag{41}$$

At last, the control block diagram of the proposed modified STO-based adaptive-gain GSTA control scheme is shown in Fig. 2.

Remark 6: A dual-loop control structure is utilized in this work (given the hypothesis that the capacitor voltages are always balanced), that is, the inner loop and the outer loop. Note that, the dynamic of the power tracking loop is always considered to be much faster than the dynamic of the voltage regulation loop according to *Assumption* 2, which implies that these two loops are in different time-scales. Therefore, in accordance with the time-scale stability theory [33], the overall closed-loop system is stable.

TABLE I
PARAMETERS OF TEST BENCH

Description	Parameters	Values	Unites
AC voltage	v_{abc}	230	$\rm V_{rms}$
Line inductor	L	2	mH
DC-link capacitor	C	6000	μF
Reference of dc voltage	$v_{\rm dc}^*$	750	V
Reference of reactive power	q^*	0	kvar
Grid frequency	f	50	Hz
Switching frequency	$f_{\rm sw}$	6.4	kHz

IV. EXPERIMENTAL VERIFICATION

In this section, a set of comparative experiments are carried out to validate the effectiveness of the proposed method. The test bench is shown in Fig. 3, which is composed of an ac

TABLE II
PARAMETERS OF DIFFERENT CONTROLLERS

Controller	Power tracking loop	Voltage regulation loop	Voltage balancing loop
ESO-STA	α_p=α_q=2.02e−6, β_p=β_q=2.27e−5 l_p=l_q=13	α_d=7, β_d=5120, l_d=16 k_3=6.6, k_4=450	k_{pb}=5e−3 k_{ib}=1e−5
STO-GSTA	α_p=α_q=1.42e−6, β_p=β_q=1e−3 μ_p=μ_q=0.01, l_p=l_q=13	α_d=6, β_d=2, μ_d=4e−3, l_d=16 k_1=35, k_2=5e4	k_{pb}=5e−3 k_{ib}=1e−5
STO#5-GSTA	Same as above	α_d=6, β_d=2, μ_d=4e−3, l_d=16 k_1=35, k_2=12e4 (High gain)	k_{pb}=5e−3 k_{ib}=1e−5
STO-GSTA#5	Same as above	α_d=9 (High gain), β_d=2, μ_d=4e−3, l_d=16 k_1=35, k_2=5e4	k_{pb}=5e−3 k_{ib}=1e−5
MSTO-AGSTA	$\alpha_{pm,qm}$=1.42e−6, $k_{p,q}$=5.34e−4, $\omega_{p,q}$=350 $\mu_{p,q}$=0.01, $\eta_{p,q}$=1.82e−6, $\varepsilon_{p,q}$=551	α_{dm}=3, k_d=650, ω_d=800, η_d=3, ε_d=0.66 μ_d=4e−3, k_1=35, k_2=5e4, k_3=1.6, k_4=200	k_{pb}=5e−3 k_{ib}=1e−5

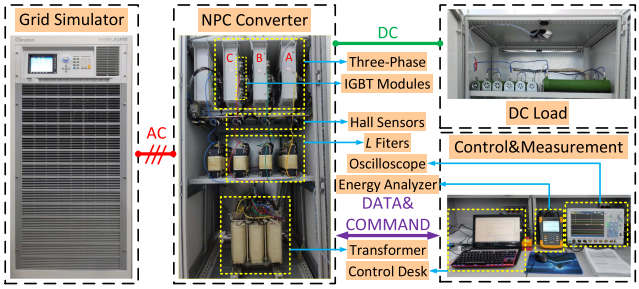

Fig. 3. Laboratory prototype of three-phase NPC converter.

power supply to emulate the ac grid, a three-level NPC rectifier, and several dc loads to emulate the external disturbances. The parameters of the test bench are given in Table I.

Two representative control strategies are also implemented serving as the comparative objects in the experiments, which consists in LESO-based STA control method (LESO-STA) and STO-based GSTA control method (STO-GSTA). The proposed modified STO-based adaptive-gain GSTA control strategy is abbreviated to MSTO-AGSTA in this section. It should be noted that the "sign" function used in fixed-gain sliding-mode controllers (STA and GSTA) are replaced by "sat" function to mitigate the chattering phenomenon in the experiments, which is indicated as

$$\mathrm{sat}(s) = \begin{cases} s/l, & \text{if } |s| \le l \\ \mathrm{sign}(s), & \text{if } |s| > l \end{cases} \tag{42}$$

where l is the boundary layer to be designed.

Note that, to assure a fair comparison, all the algorithms are tuned to the proper performance, and the principle of the tuning strategy is to improve the dynamic performance and the disturbance rejection ability of the system as much as possible without affecting the steady-state performance of the system. In addition, the performance of the STO-GSTA approach with high gains is also given in the comparative experiments to further evaluate the performance of this method and the proposed one. Finally, in order to verify that the proposed MSTO-AGSTA controller overcomes the tradeoff between dynamic response and chattering, providing better dynamic, steady-state performance, and disturbance rejection ability simultaneously, the performance of the STO-GSTA approach with a sweep of control parameters is also presented and compared with the proposed method.

TABLE III
STO-GSTA CONTROLLER WITH DIFFERENT OBSERVER GAINS

	STO#1-GSTA	STO#2-GSTA	STO#3-GSTA	STO#4-GSTA
(k_1, k_2)	(35, 6.4e4)	(35, 7.8e4)	(35, 9.2e4)	(35, 10.6e4)

TABLE IV
STO-GSTA CONTROLLER WITH DIFFERENT CONTROLLER GAINS

	STO-GSTA#1	STO-GSTA#2	STO-GSTA#3	STO-GSTA#4
(α_d, β_d)	(6.6, 2)	(7.2, 2)	(7.8, 2)	(8.4, 2)

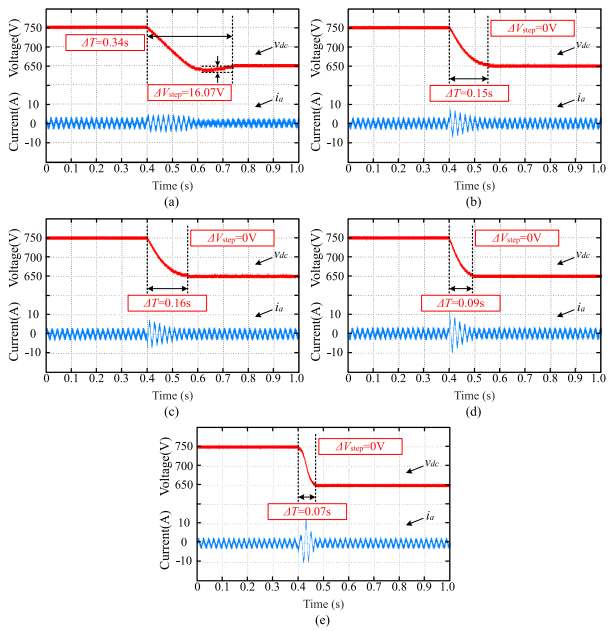

Fig. 4. Transient responses of NPC DC-link voltage under a voltage step from 750 to 650 V based on different control strategies. (a) LESO-STA. (b) STO-GSTA. (c) STO#5-GSTA. (d) STO-GSTA#5. (e) Proposed MSTO-AGSTA.

A. Comparative Study Among LESO-STA, STO-GSTA, and Proposed MSTO-AGSTA Methods

In this section, the proposed MSTO-AGSTA control scheme is compared with LESO-STA, STO-GSTA, and STO-GSTA with high gains, i.e., STO#5-GSTA and STO-GSTA#5. Note that, the suffix #n ($n = 1, \cdots, 5$) denotes the observer/controller in the voltage regulation loop using high gains, and the other

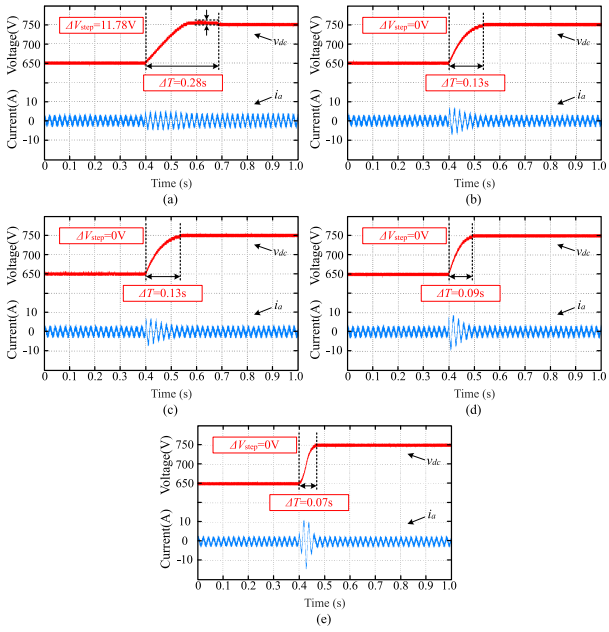

Fig. 5. Transient responses of NPC DC-link voltage under a voltage step from 650 to 750 V based on different control strategies. (a) LESO-STA. (b) STO-GSTA. (c) STO#5-GSTA. (d) STO-GSTA#5. (e) Proposed MSTO-AGSTA.

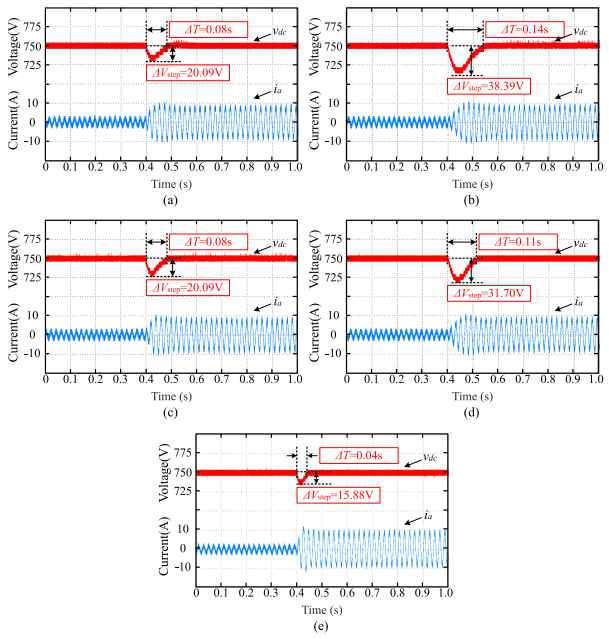

Fig. 6. NPC DC-link voltage waveforms under a 150 Ω load step based on different control strategies. (a) LESO-STA. (b) STO-GSTA. (c) STO#5-GSTA. (d) STO-GSTA#5. (e) Proposed MSTO-AGSTA.

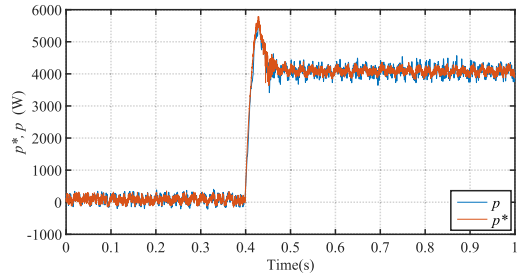

Fig. 7. Waveforms of active power p and its reference p^* under a 150 Ω load step based on proposed MSTO-AGSTA method.

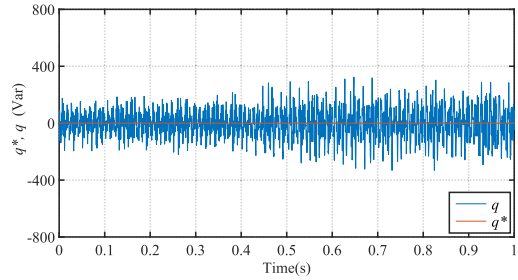

Fig. 8. Waveforms of reactive power q and its reference q^* under a 150 Ω load step based on proposed MSTO-AGSTA method.

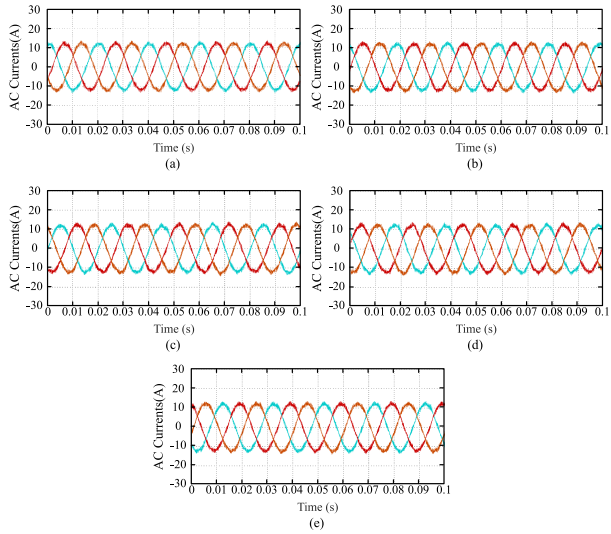

Fig. 9. Three-phase AC current waveforms with a 5.3 kW power transmission based on different control strategies. (a) LESO-STA. (b) STO-GSTA. (c) STO#5-GSTA. (d) STO-GSTA#5. (e) Proposed MSTO-AGSTA.

parameters are exactly the same as the original one. The higher the value of n is, the higher the gain of the observer/controller used. The control parameters of these controllers are shown in Tables II–IV.

At first, the dynamic performance are evaluated. The transient responses of the dc voltage under a voltage step from 750 to 650 V and a voltage step from 650 to 750 V are shown in Figs. 4 and 5, respectively. Clearly, the proposed MSTO-AGSTA control scheme achieves the best dynamic performance among these controllers. It prevents voltage overshoot and the settling times are both only 0.07 s in the dynamic performance tests, which, respectively, reduces by around 79% and 53% compared with the LESO-STA and STO-GSTA in voltage sag test, and, respectively, reduces by around 75% and 46% compared with the LESO-STA and STO-GSTA in voltage swell test. On the other hand, it can be observed that the transient response of STO-GSTA control method can be improved by

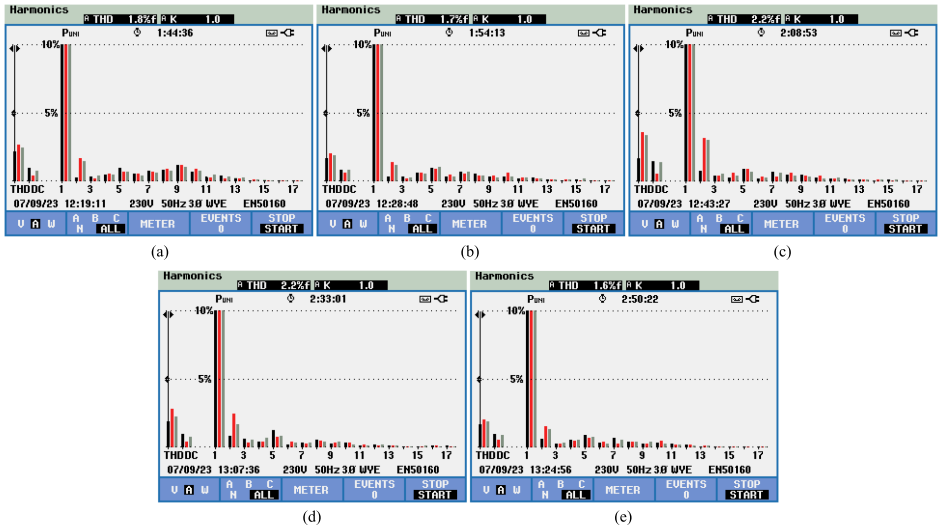

Fig. 10. Three-phase AC current harmonic spectrums with a 5.3 kW power consumption based on different control strategies. (a) LESO-STA. (b) STO-GSTA. (c) STO#5-GSTA. (d) STO-GSTA#5. (e) Proposed MSTO-AGSTA.

using high gains in GSTA. However, its steady-state performance is sacrificed due to the increased chattering, which will be presented later.

Afterwards, the ability to resist disturbance of different controllers are tested. Fig. 6 shows the NPC dc-link voltage waveforms under a 150 Ω load step based on different control strategies. It can be seen that the proposed MSTO-AGSTA control scheme also has advantage over others in the disturbance rejection ability. The droop voltage of the proposed method is only 15.88 V under a 150 Ω load step, which, respectively, reduces by around 21% and 59% compared with the LESO-STA and STO-GSTA, and the settling time of the proposed method is merely 0.04 s, which, respectively, reduces by around 50% and 71% compared with the LESO-STA and STO-GSTA. By combining the attractive features of LESO and STO, the MSTO provides rather high disturbance rejection ability against exogenous perturbations. On the other hand, the responses of active and reactive power based on the proposed MSTO-AGSTA method are also presented, which are shown in Figs. 7 and 8. It can be seen that both active power and reactive power can track their references accurately.

Finally, the steady-state performance is evaluated under the condition that the NPC converter is operated with a 5.3 kW power consumption (two dc loads are connected in parallel in the dc side, and $R_1 = 150\,\Omega$, $R_2 = 360\,\Omega$). The corresponding NPC ac current waveforms and harmonic spectra are shown in Figs. 9 and 10. It can be observed that the proposed MSTO-AGSTA control scheme achieves a better total harmonic distortion (THD) of the ac currents compared with others. In addition, it is clear that although the STO-GSTA#5 and STO#5-GSTA controllers provide good dynamic performance and disturbance rejection ability, respectively, the ac current quality is sacrificed due to the increased chattering.

To summarize, the proposed MSTO-AGSTA control scheme simultaneously achieves the best disturbance rejection ability, dynamic, and steady-state performance among these methods.

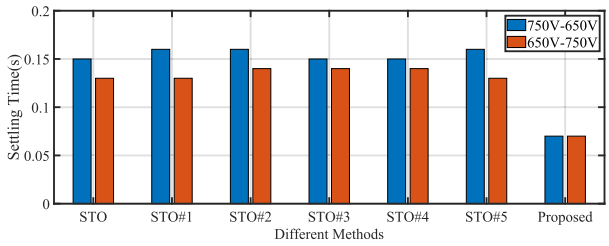

Fig. 11. Settling time of NPC DC-link voltage under a voltage step from 750 to 650 V and 650 to 750 V based on different control strategies.

B. Comparative Study Among STO-GSTA Method With Increasing Gains and Proposed MSTO-AGSTA Methods

According to the experimental results given in Section IV-A, a tradeoff exists between the steady-state performance and the dynamic performance as well as the disturbance rejection ability in the STO-GSTA controller, and the proposed MSTO-AGSTA method overcomes this issue. In this section, to further validate this point, not only one specific high gain, but a sweep of high gains are applied in the STO-GSTA controller. The performances are shown and compared with the proposed MSTO-AGSTA control scheme. The parameters of the STO-GSTA controller with increasing gains are shown in Tables III and IV.

A set of identical tests are carried out based on the STO-GSTA controller with increasing observer gains, including the evaluations of dynamic and steady-state performance, as well as disturbance rejection ability. Note that, in the dynamic performance test, only the settling time of different approaches is drawn with bar charts since there are no overshoot voltage for all these methods in this test. With increasing observer gains, the transient responses of the STO-GSTA controller almost remain the same and the disturbance rejection abilities are enhanced according to Figs. 11 and 12. However, the THD values are increasing according to Fig. 13, which implies that the steady-state

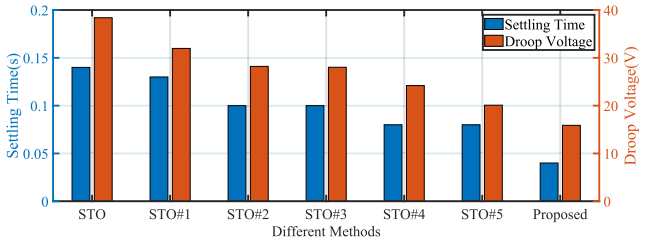

Fig. 12. Settling time and voltage dip of NPC DC-link voltage under a 150 Ω load step based on different control strategies.

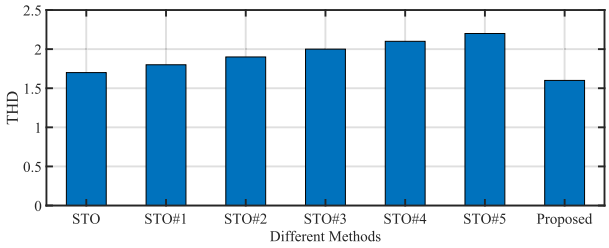

Fig. 13. Three-phase AC current THD with a 5.3 kW power consumption based on different control strategies.

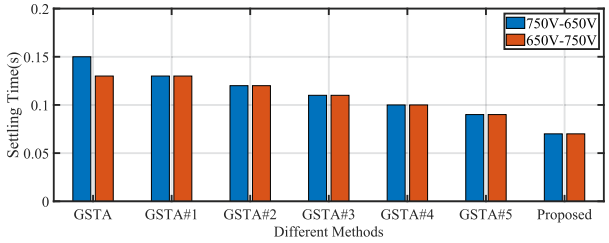

Fig. 14. Settling time of NPC DC-link voltage under a voltage step from 750 to 650 V and 650 to 750 V based on different control strategies.

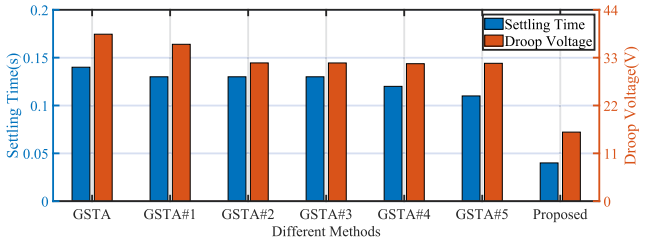

Fig. 15. Settling time and voltage dip of NPC DC-link voltage under a 150 Ω load step based on different control strategies.

performance is sacrificed due to the increased chattering induced by increased observer gains in STO.

On the other hand, similar experiments are implemented based on the STO-GSTA controller with increasing controller gains, which are shown in Figs. 14–16. Note that, in the dynamic performance test, only the settling time of different approaches is drawn with bar charts since there are no overshoot voltage for all these methods in this test. Clearly, with increasing controller gains, the transient responses, and disturbance rejection abilities of the STO-GSTA controller are both improved according to the results given in Figs. 14 and 15. Nevertheless, the THD values

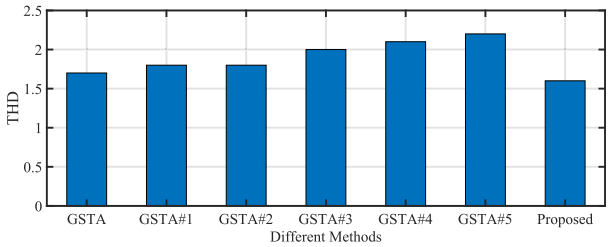

Fig. 16. Three-phase AC current THD with a 5.3 kW power consumption based on different control strategies.

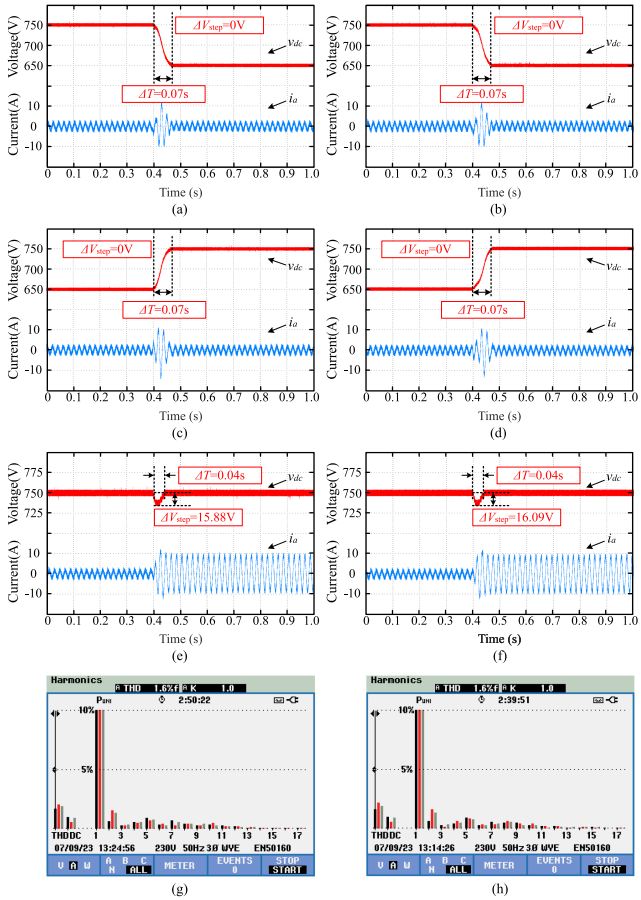

Fig. 17. Dynamic, steady state, and disturbance rejection performance of the proposed MSTO-AGSTA method when the inductance L and capacitance C both have -10% variation. (a) Voltage step from 750 to 650 V. (b) Voltage step from 750 to 650 V under parameter variation. (c) Voltage step from 650 to 750 V. (d) Voltage step from 650 to 750 V under parameter variation. (e) Load step (150 Ω). (f) Load step (150 Ω) under parameter variation. (g) Current harmonic spectra for a 5.3 kW active power consumption. (h) Current harmonic spectra for a 5.3 kW active power consumption under parameter variation.

are also increasing in accordance with Fig. 16, which means that the high gains provide fast transient and enhanced robustness at the expense of bad steady-state performance due to increased chattering.

Consequently, according to the results given in Figs. 11–16, it is obvious that compared with the STO-GSTA control strategy, the proposed MSTO-AGSTA method overcomes the tradeoff between chattering and dynamic performance, which achieves

the better disturbance rejection ability, dynamic, and steady-state performance simultaneously.

C. Robustness Evaluation of Proposed MSTO-AGSTA Method Under Parameter Variation

In this part, the robustness of the proposed MSTO-AGSTA method under parameter variation is tested. The performance of this method under parameter uncertainties is presented in Fig. 17, where the value of the inductor L and capacitor C both have -10% variation in the control implementation. It can be observed that the performance of the proposed method almost remains the same in the presence of parameter variation, which verifies the robustness of the proposed method even under parameter uncertainties.

V. Conclusion

In this work, a modified STO-based adaptive-gain GSTA is proposed for NPC converters to enhance the performance. In order to overcome the tradeoff between chattering phenomenon and transient response, an adaptive law is introduced for the standard GSTA. By applying the adaptive-gain GSTA to NPC converters, the dynamic and steady-state performance are enhanced simultaneously. Additionally, a modified STO is added in the voltage regulator to reject external unknown disturbances. Compared to the conventional STO and LESO, this one not only provides finite-time convergence, but also achieves a fast disturbance estimation even when a large estimation error appears. The proposed method is validated and compared with other existing algorithms based on a real scale three-level NPC converter, including the LESO-based STA and STO-based GSTA. In the dynamic performance tests, the proposed method prevents voltage overshoot and reduces the settling times by around 75% and 46% compared with the LESO-STA and STO-GSTA. In the disturbance rejection tests, the proposed method reduces the droop voltage by around 21% and 59% compared with the LESO-STA and STO-GSTA, and reduces the settling time by around 50% and 71%. Finally, several comparative studies among STO-based GSTA with increasing gains and the proposed method are carried out, and the results confirm that the proposed modified STO-based adaptive-gain GSTA control scheme overcomes the tradeoff between chattering and transient response, and it is superior to the other controllers in dynamic and steady-state performance as well as disturbance rejection ability simultaneously.

Appendix

The proof of Proposition 1 is analogous to the proof of [31, Th. 1]. Here only some details that are different from the proof in [31] are introduced to facilitate the understanding of the proof of Proposition 1:

The Lyapunov function is selected as [31]

$$V(s_d)=\underbrace{\zeta^T P\zeta}_{V_1}+\underbrace{\frac{1}{2\gamma_1}(\alpha_d-\alpha_d^*)^2+\frac{1}{2\gamma_2}(\beta_d-\beta_d^*)^2}_{V_2} \tag{43}$$

where

$$\zeta=\begin{bmatrix}\zeta_1\\ \zeta_2\end{bmatrix}=\begin{bmatrix}\phi_1(s_d)\\ \omega_d\end{bmatrix},\quad P=\begin{bmatrix}\lambda+4\varepsilon^2 & -2\varepsilon\\ -2\varepsilon & 1\end{bmatrix}. \tag{44}$$

Then, the time derivative of ζ can be deduced as

$$\begin{aligned}\dot\zeta&=\begin{bmatrix}\phi_1'(s_d)\left(-\alpha_d b_d\phi_1(s_d)+\omega_d\right)\\ -\beta_d b_d\phi_1(s_d)\phi_1'(s_d)+\dot a_{de}\end{bmatrix}\\&=\phi_1'(s_d)\begin{bmatrix}-\alpha_d b_d & 1\\ -\beta_d b_d & 0\end{bmatrix}\begin{bmatrix}\zeta_1\\ \zeta_2\end{bmatrix}+\phi_1'(s_d)\begin{bmatrix}0\\ \frac{1}{\phi_1'(s_d)}\dot a_{de}\end{bmatrix}\end{aligned} \tag{45}$$

where $\phi_1'(s_d)=\frac{1}{2}|s_d|^{-1/2}+\mu_d$.

According to *Assumption* 3, it can be deduced that

$$|\dot a_{de}|\le 2\delta_{d1}\left(\frac{1}{2}+\frac{3}{2}\mu_d|s_d|^{1/2}+\mu_d^2|s_d|\right) \tag{46}$$

then the functions $\dot a_{de}$ can be written as

$$\begin{aligned}\dot a_{de}&=\rho\left(\frac{1}{2}+\frac{3}{2}\mu_d|s_d|^{1/2}+\mu_d^2|s_d|\right)\operatorname{sign}(s_d)\\&=\rho\phi_1'(s_d)\zeta_1\end{aligned} \tag{47}$$

where ρ is a function with following boundaries

$$0<\rho\le 2\delta_{d1}. \tag{48}$$

Substituting (47) into (45) yields

$$\dot\zeta=\phi_1'(s_d)A\zeta \tag{49}$$

where

$$A=\begin{bmatrix}-\alpha_d b_d & 1\\ -\beta_d b_d+\rho & 0\end{bmatrix}. \tag{50}$$

Then, the time derivative of V_1 can be derived as

$$\dot V_1=\dot\zeta^T P\zeta+\zeta^T P\dot\zeta=-\phi_1'(s_d)\zeta^T Q\zeta \tag{51}$$

where

$$Q=-(A^TP+PA)=\begin{bmatrix}Q_1 & Q_2\\ Q_3 & Q_4\end{bmatrix} \tag{52}$$

with

$$\begin{aligned}Q_1&=2\alpha_d b_d\lambda+4\varepsilon\rho+4\varepsilon b_d(2\varepsilon\alpha_d-\beta_d)\\Q_2&=Q_3=-\lambda-4\varepsilon^2+b_d(\beta_d-2\varepsilon\alpha_d)-\rho\\Q_4&=4\varepsilon.\end{aligned} \tag{53}$$

Similar as [31], the control gain β_d is defined as $\beta_d=2\varepsilon\alpha_d$, and to assure the positive definiteness of Q, its minimal eigenvalue satisfies $\lambda_{\min}(Q)\ge 2\varepsilon$, then it can be deduced that

$$\alpha_d>\frac{\left(\lambda+4\varepsilon^2\right)^2+4\varepsilon\delta_{d1}^2+4\delta_{d1}\lambda+4\varepsilon^2}{4\varepsilon\lambda b_d}. \tag{54}$$

Afterwards, the time derivative of V_1 can be deduced as

$$\begin{aligned}\dot V_1&\le-\phi_1'(s_d)\lambda_{\min}\{Q\}\|\zeta\|_2^2\\&=-\frac{1}{2|s_d|^{\frac{1}{2}}}\lambda_{\min}\{Q\}\|\zeta\|_2^2-\mu_d\lambda_{\min}\{Q\}\|\zeta\|_2^2\end{aligned}$$

$$\leq -\varepsilon\|\zeta\|_2 - 2\varepsilon\mu_d\|\zeta\|_2^2$$
$$\leq -\varepsilon\frac{V_1^{\frac{1}{2}}(s_d)}{\lambda_{\max}^{\frac{1}{2}}\{P\}} - 2\varepsilon\mu_d\frac{V_1(s_d)}{\lambda_{\max}\{P\}}$$
$$\leq -r_1 V_1^{\frac{1}{2}} - r_2 V_1 \tag{55}$$

where

$$r_1 = \varepsilon\frac{\lambda_{\min}^{\frac{1}{2}}\{P\}}{\lambda_{\max}\{P\}}, \quad r_2 = \frac{2\varepsilon\mu_d}{\lambda_{\max}\{P\}}. \tag{56}$$

Afterwards, following [31, proof of Theorem 1], it can be finally proved that a 2-sliding mode is established in finite time via the GSTA (19) with time-varying gains (22).

REFERENCES

[1] J. Pontt, J. Rodriguez, and R. Huerta, "Mitigation of noneliminated harmonics of SHEPWM three-level multipulse three-phase active front end converters with low switching frequency for meeting standard IEEE-519-92," *IEEE Trans. Power Electron.*, vol. 19, no. 6, pp. 1594–1600, Nov. 2004.

[2] B. Chikondra, U. R. Muduli, and R. K. Behera, "Improved DTC technique for THL-NPC VSI fed five-phase induction motor drive based on VVs assessment over a wide speed range," *IEEE Trans. Power Electron.*, vol. 37, no. 2, pp. 1972–1981, Feb. 2022.

[3] T. Dragičević, X. Lu, J. C. Vasquez, and J. M. Guerrero, "DC microgrids—Part II: A review of power architectures, applications, and standardization issues," *IEEE Trans. Power Electron.*, vol. 31, no. 5, pp. 3528–3549, May 2016.

[4] X. Xu, Z. Zheng, K. Wang, B. Yang, and Y. Li, "A carrier-based common-mode voltage elimination method for back-to-back three-level NPC converters," *IEEE Trans. Power Electron.*, vol. 37, no. 3, pp. 3040–3052, Mar. 2022.

[5] S. Vazquez, P. Acuna, R. P. Aguilera, J. Pou, J. I. Leon, and L. G. Franquelo, "DC-link voltage-balancing strategy based on optimal switching sequence model predictive control for single-phase H-NPC converters," *IEEE Trans. Ind. Electron.*, vol. 67, no. 9, pp. 7410–7420, Sep. 2020.

[6] K. Kumari and A. K. Jain, "Performance assessment of three phase NPC based grid integrated single stage solar PV system with reduced dc-bus capacitor," *IEEE Trans. Ind. Electron.*, vol. 70, no. 4, pp. 3773–3781, Apr. 2023.

[7] A. Tcai, Y. Kwon, S. Pugliese, and M. Liserre, "Reduction of the circulating current among parallel NPC inverters," *IEEE Trans. Power Electron.*, vol. 36, no. 11, pp. 12504–12514, Nov. 2021.

[8] T. Dragicevic, S. Vazquez, and P. Wheeler, "Advanced control methods for power converters in DG systems and microgrids," *IEEE Trans. Ind. Electron.*, vol. 68, no. 7, pp. 5847–5862, Jul. 2021.

[9] F. Blaabjerg, R. Teodorescu, M. Liserre, and A. Timbus, "Overview of control and grid synchronization for distributed power generation systems," *IEEE Trans. Ind. Electron.*, vol. 53, no. 5, pp. 1398–1409, Oct. 2006.

[10] J. Rocabert, A. Luna, F. Blaabjerg, and P. Rodríguez, "Control of power converters in AC microgrids," *IEEE Trans. Power Electron.*, vol. 27, no. 11, pp. 4734–4749, Nov. 2012.

[11] Z. Liu et al., "A novel faster fixed-time adaptive control for robotic systems with input saturation," *IEEE Trans. Ind. Electron.*, to be published, doi: 10.1109/TIE.2023.3281701.

[12] X. Shen et al., "Adaptive second-order sliding mode control for grid-connected NPC converters with enhanced disturbance rejection," *IEEE Trans. Power Electron.*, vol. 37, no. 1, pp. 206–220, Jan. 2022.

[13] Y. Gui, F. Blaabjerg, X. Wang, J. D. Bendtsen, D. Yang, and J. Stoustrup, "Improved DC-link voltage regulation strategy for grid-connected converters," *IEEE Trans. Ind. Electron.*, vol. 68, no. 6, pp. 4977–4987, Jun. 2021.

[14] F. Sebaaly, H. Vahedi, H. Y. Kanaan, N. Moubayed, and K. Al-Haddad, "Design and implementation of space vector modulation-based sliding mode control for grid-connected 3L-NPC inverter," *IEEE Trans. Ind. Electron.*, vol. 63, no. 12, pp. 7854–7863, Dec. 2016.

[15] X. Shen et al., "High-performance second order sliding mode control for NPC converters," *IEEE Trans. Ind. Informat.*, vol. 16, no. 8, pp. 5345–5356, Aug. 2020.

[16] J. Lu, M. Savaghebi, A. M. Y. Mohammad Ghias, X. Hou, and J. M. Guerrero, "A reduced-order generalized proportional integral observer-based resonant super-twisting sliding mode control for grid-connected power converters," *IEEE Trans. Ind. Electron.*, vol. 68, no. 7, pp. 5897–5908, Jul. 2021.

[17] Y. Yin et al., "Observer-based sliding-mode control for grid-connected power converters under unbalanced grid conditions," *IEEE Trans. Ind. Electron.*, vol. 69, no. 1, pp. 517–527, Jan. 2022.

[18] C. Gong, W. K. Sou, and C. S. Lam, "Second-order sliding-mode current controller for LC-coupling hybrid active power filter," *IEEE Trans. Ind. Electron.*, vol. 68, no. 3, pp. 1883–1894, Mar. 2021.

[19] J. A. Moreno, "A linear framework for the robust stability analysis of a generalized super-twisting algorithm," in *Proc. 6th Int. Conf. Elect. Eng., Comput. Sci. Autom. Control*, 2009, pp. 1–6.

[20] I. L. G. Borlaug, K. Y. Pettersen, and J. T. Gravdahl, "Tracking control of an articulated intervention autonomous underwater vehicle in 6DOF using generalized super-twisting: Theory and experiments," *IEEE Trans. Control Syst. Technol.*, vol. 29, no. 1, pp. 353–369, Jan. 2021.

[21] C. Fu, C. Zhang, G. Zhang, J. Song, C. Zhang, and B. Duan, "Disturbance observer-based finite-time control for three-phase AC–DC converter," *IEEE Trans. Ind. Electron.*, vol. 69, no. 6, pp. 5637–5647, Jun. 2022.

[22] J. Lu, S. Golestan, M. Savaghebi, J. C. Vasquez, J. M. Guerrero, and A. Marzabal, "An enhanced state observer for DC-link voltage control of three-phase AC/DC converters," *IEEE Trans. Power Electron.*, vol. 33, no. 2, pp. 936–942, Feb. 2018.

[23] L. Zhao, C. Zheng, Y. Wang, and B. Liu, "A finite-time control for a pneumatic cylinder servo system based on a super-twisting extended state observer," *IEEE Trans. Syst., Man, Cybern. Syst.*, vol. 51, no. 2, pp. 1164–1173, Feb. 2021.

[24] W. Luo, S. Vazquez, J. Liu, F. Gordillo, L. G. Franquelo, and L. Wu, "Control system design of a three-phase active front end using a sliding-mode observer," *IEEE Trans. Syst., Man, Cybern. Syst.*, vol. 52, no. 2, pp. 739–748, Feb. 2022.

[25] J. A. Moreno and M. Osorio, "A Lyapunov approach to second-order sliding mode controllers and observers," in *Proc. 47th IEEE Conf. Decis. Control*, 2008, pp. 2856–2861.

[26] R. Portillo, S. Vazquez, J. I. Leon, M. M. Prats, and L. G. Franquelo, "Model based adaptive direct power control for three-level NPC converters," *IEEE Trans. Ind. Informat.*, vol. 9, no. 2, pp. 1148–1157, May 2013.

[27] A. Chalanga, S. Kamal, L. M. Fridman, B. Bandyopadhyay, and J. A. Moreno, "Implementation of super-twisting control: Super-twisting and higher order sliding-mode observer-based approaches," *IEEE Trans. Ind. Electron.*, vol. 63, no. 6, pp. 3677–3685, Jun. 2016.

[28] J. A. Moreno and M. Osorio, "Strict Lyapunov functions for the super-twisting algorithm," *IEEE Trans. Autom. Control*, vol. 57, no. 4, pp. 1035–1040, Apr. 2012.

[29] J. Davila, L. Fridman, and A. Levant, "Second-order sliding-mode observer for mechanical systems," *IEEE Trans. Autom. Control*, vol. 50, no. 11, pp. 1785–1789, Nov. 2005.

[30] Z. Gao, "Scaling and bandwidth-parameterization based controller tuning," in *Proc. Amer. Control Conf.*, 2003, vol. 6, pp. 4989–4996.

[31] Y. Shtessel, M. Taleb, and F. Plestan, "A novel adaptive-gain supertwisting sliding mode controller: Methodology and application," *Automatica*, vol. 48, no. 5, pp. 759–769, 2012.

[32] J. A. Moreno, "A Lyapunov approach to output feedback control using second-order sliding modes," *IMA J. Math. Control Inf.*, vol. 29, no. 3, pp. 291–308, 2012.

[33] F. Umbría, J. Aracil, F. Gordillo, F. Salas, and J. A. Sánchez, "Three-time-scale singular perturbation stability analysis of three-phase power converters," *Asian J. Control*, vol. 16, no. 5, pp. 1361–1372, 2014.

Xiaoning Shen (Member, IEEE) was born in Anhui, China, in 1995. He received the M.S. degree in electrical engineering from the Harbin Institute of Technology, Shenzhen, China, in 2017, and the Ph.D. degree in control science and engineering from the Harbin Institute of Technology, Harbin, China, in 2022.

Since 2022, he has been an Assistant Professor with the Harbin Institute of Technology, Harbin, China. His current research interests include sliding-mode control, observation methods, and their applications to power electronic systems.

Chengwei Wu (Member, IEEE) received the B.S. degree in management from the Arts and Science College, Bohai University, Jinzhou, China, in 2013, the M.S. degree in software engineering from Bohai University, Jinzhou, China, in 2016, and the Ph.D. degree in control science and engineering from the Harbin Institute of Technology, Harbin, China, in 2021.

From July 2015 to December 2015, he was a Research Assistant with the Department of Mechanical Engineering, The Hong Kong Polytechnic University, Hong Kong. From 2019 to 2021, he was a joint-Ph.D. student with the Department of Cognitive Robotics, Delft University of Technology, Delft, The Netherlands. He is currently an Assistant Professor with the Harbin Institute of Technology, Harbin, China. His research interests include reinforcement learning, sliding-mode control, and cyber-physical systems.

Zhuang Liu (Graduate Student Member, IEEE) received the B.S. degree in electrical engineering and automation in 2017 from the China University of Mining and Technology, Xuzhou, China, and the M.E. degree in electrical engineering in 2019 from the Harbin Institute of Technology, Harbin, China, where he is currently working toward the Ph.D. degree in control science and engineering.

His current research interests include adaptive control, sliding-mode control, neural network control, fuzzy logic system, model predictive control, finite-time control, fixed-time control, and their applications to robotics and power electronic systems.

Yijie Wang (Senior Member, IEEE) was born in Heilongjiang Province, China, in 1982. He received the B.S., M.S., and Ph.D. degrees in electrical engineering from the Harbin Institute of Technology, Harbin, China, in 2005, 2007, and 2012, respectively.

From 2012 to 2014, he was a Lecturer with the Department of Electrical and Electronics Engineering, Harbin Institute of Technology. From 2014 to 2017, he was an Associate Professor with the Department of Electrical and Electronics Engineering, Harbin Institute of Technology. Since 2017, he has been a Professor with the Department of Electrical and Electronics Engineering, Harbin Institute of Technology. His interests include dc–dc converters, soft-switching power converters, power factor correction circuits, digital control electronic ballasts, LED lighting systems.

Dr. Wang is currently an Associate Editor for IEEE TRANSACTIONS ON INDUSTRIAL ELECTRONICS, IEEE JOURNAL OF EMERGING AND SELECTED TOPICS IN POWER ELECTRONICS, IEEE ACCESS, *IET Power Electronics*, and *Journal of Power Electronics*.

Jose I. Leon (Fellow, IEEE) was born in Cadiz, Spain. He received the B.S., M.S., and Ph.D. degrees in telecommunications engineering from Universidad de Sevilla, Seville, Spain, in 1999, 2001, and 2006, respectively.

He is currently an Associate Professor with Universidad de Sevilla with ENGREEN. Since 2019, he has also been a Chair Professor with the Department of Control Science and Engineering, Harbin Institute of Technology, Harbin, China. His research interests include modulation and control of power converters for high-power applications and renewable energy systems.

Dr. Leon was a corecipient of the 2008, 2015, 2020, and 2022 Best Paper Award of *IEEE Industrial Electronics Magazine*, and the 2012 Best Paper Award of the IEEE TRANSACTIONS ON INDUSTRIAL ELECTRONICS. He was the recipient of the 2014 IEEE J. David Irwin Industrial Electronics Society Early Career Award, the 2017 IEEE Bimal K. Bose Energy Systems Award, and the 2017 Manuel Losada Villasante Award for excellence in research and innovation.

Jianxing Liu (Senior Member, IEEE) received the B.S. degree in mechanical engineering and the M.E. degree in control science and engineering from the Harbin Institute of Technology, Harbin, China, in 2004 and 2010, respectively, and the Ph.D. degree in automation from the University of Technology of Belfort-Montbeliard, Belfort, France, in 2014.

Since 2014, he has been with the Harbin Institute of Technology, where he is currently a Professor with the Department of Control Science and Engineering. His current research interests include sliding-mode control, intelligent systems and robot technologies, and industrial electronic systems.

Dr. Liu is on the Data Driven Control and Monitoring Technical Committee of the IEEE Industrial Electronics Society and is currently an Associate Editor for several journals, including IEEE TRANSACTIONS ON CIRCUITS AND SYSTEMS II: EXPRESS BRIEFS, IEEE SYSTEMS JOURNAL, NONLINEAR DYNAMICS, *ISA Transactions*, and IEEE JOURNAL OF EMERGING AND SELECTED TOPICS IN INDUSTRIAL ELECTRONICS. He is also an Associate Editor for the Conference Editorial Board, IEEE Control Systems Society. He was named as the Highly Cited Researcher from 2019 to 2022.

Leopoldo G. Franquelo (Life Fellow, IEEE) was born in Malaga, Spain. He received the M.Sc. and Ph.D. degrees in electrical engineering from the Universidad de Sevilla, Seville, Spain, in 1977 and 1980, respectively.

He was an Associate Professor from 1982 to 1986 with the Electronics Engineering Department, Sevilla University, Seville, Spain, and is currently a Professor with the Electronics Engineering Department, Sevilla University, since 1986 and a Professor with the Department of Control Science and Engineering, Harbin Institute of Technology, Harbin, China, since 2016. He has participated in more than 100 Industrial and R&D projects and was authored or coauthored more than 300 papers, 108 of them in IEEE Journals, and 25 of them in IEEE Magazines. His current research interests include modulation techniques for multilevel inverters and application to power electronic systems for renewable energy systems.

Dr. Franquelo is an IEEE Fellow since 2005 and an IEEE Industrial Electronics Society (IES) Distinguished Lecturer since 2006. In the IEEE TRANSACTION INDUSTRIAL ELECTRONICS, he became an Associate Editor in 2007, Co-Editor-in-Chief in 2014, and the Editor-in-Chief 2016–2018. He is currently is an Editor-in-Chief of the IEEE Open Journal of the Industrial Electronics Society. He was a Member-at-Large of the IES AdCom (2002–2003), Vice President for Conferences (2004–2007), and President Elect of the IES (2008–2009). He was the President of the IES (2010–2011) and is an IES AdCom Life member. In 2009 and 2013, he was the recipient of the prestigious Andalusian Research Award and FAMA Award recognizing the excellence of his research career. He was also the recipient of a number of Best Paper Awards from IEEE journals and Eugene Mittelmann Outstanding Research Achievement Award and the Antohny J. Hornfeck Service Award from IEEE-IES in 2012 and 2015, respectively.